Proceedings of the 26th Annual International Conference of the IEEE EMBS
San Francisco, CA, USA • September 1-5, 2004

# Touchless Monitoring of Breathing Function

Ramya Murthy*, Ioannis Pavlidis†, and Panagiotis Tsiamyrtzis‡
* Department of Computer Science, University of Houston, Houston, Texas
Email: rnmurthy@mail.uh.edu
† Department of Computer Science, University of Houston, Houston, Texas
Email: ipavlidi@mail.uh.edu
‡Department of Statistics, University of Athens, Athens, Greece
Email: pt@aueb.gr

*Abstract*— **We have developed a novel method for non-contact measurement of breathing function. The method is based on statistical modeling of dynamic thermal data captured through an infrared imaging system. The expired air has higher temperature than the typical background of indoor environments (e.g., walls). Therefore, the particles of the expired air emit at a higher power than the background, a phenomenon which is captured as a distinct thermal signature in the infrared imagery. There is significant technical difficulty in computing this signature, however, because the phenomenon is of very low intensity and transient nature. We use an advanced statistical algorithm based on the method of moments and the Jeffrey's divergence measure to address the problem. So far, we were able to compute correctly the breathing waveforms for ten (10) subjects at distances ranging from 6-8 feet. The results were checked against concomitant ground-truth data collected with a traditional contact sensor. The technology is expected to find applications in the next generation of touchless polygraphy and in preventive health care.**

## I. Introduction

Monitoring of breathing function has applications among others in polygraphy, sleep studies, sport training, preventing sudden death syndrome in neonates, and patient monitoring. Various contact measurement methods have been developed for estimating the breathing rate of a subject. George B. Moody, *et al.* developed a contact modality in which numerous Electrocardiogram (ECG) electrodes and sensors are attached to the subject [1]. The principle of operation is based on the fact that the heart rate is typically modulated by breathing, a phenomenon known as sinus arrhythmia [2]. Therefore, a signal corresponding to the heart function contains breath information, which is filtered out using band-pass filters.

As an improvement over the ECG method, the BioMatt method [3] was developed in Finland by a group of researchers who were studying sleep disorders. BioMatt performs measurements of vital signs, such as breathing and cardiac activity without electrodes. Initially, BioMatt could not distinguish motion that was due to breathing versus cardiac activity or body movement. Later, Larson developed a signal processing technique to separate out the components of the BioMatt signal [4].

The nasal temperature probe [5] is another contact modality, which contains a thermistor measuring nasal air temperature variation as an indication of breathing. The abdominal strain gauge transducer [6], which is strapped around the subject's chest, measures the change in thoracic or abdominal circumference while breathing. The disadvantage of all the aforementioned technologies is that they require close contact with the subject, which in certain cases may be quite uncomfortable and awkward (e.g., abdominal transducer).

A more subject-friendly method is photoplethysmography [7], where near-infrared light is emitted into the skin. The amount of backscattered light corresponds to the variation of the blood volume. As in ECG, the breath waveform is separated from the cardiac signal. However, using heart function as a basis for acquiring the breathing waveform is unreliable since sinus arrhythmia is not present in all individuals. Control of cardiac activity by breathing depends on the age and medications administered to subjects.

A touchless but active technology called Radar Vital Signs Monitor (RVSM) [8] was developed in 1996 to monitor the performance of Olympic athletes. The RVSM measures breath at distances of up to 15 feet behind an 8 inch hollow concrete or wooden wall. It detects breathing-induced movement of the chest based on the Doppler effect. The disadvantage of this technique is that motion artifacts corrupt breath signals.

In 2000, infrared imaging proved its potential in deception detection when thermal image analysis was used by Pavlidis *et al.* to detect facial patterns of stress at a distance [9]. A little later Pavlidis *et al.* used thermal imaging to compute periorbital perfusion as a replacement of the corresponding polygraph channel that uses finger contact sensing [10]. The proposed use of infrared imaging for computing breathing function may also replace the corresponding polygraph channel that uses abdominal transducing. Incremental replacement of contact channels may prove very effective in the field of polygraphy, where it is essential that subjects feel as comfortable as possible during examination.

In this paper, we describe a second-order statistical method to estimate in a contact-free manner the breathing rate of human subjects using thermal video sequences. We provide a brief overview of breathing physiology in Section II. In Section III we describe how we select and track the region of interest in the scene, where our breathing computation applies. In Section IV we describe the statistical computation that we employ to determine the breathing rate. In Sections V and VI we discuss the experimental setup and results respectively. We conclude the paper in Section VII.

0-7803-8439-3/04/$20.00©2004 IEEE

## II. Breathing Function

In our study, we are interested in monitoring breathing using infrared imaging. The breathing cycle consists of inspiration, expiration, and post-expiratory pause [11]. During quiet breathing, inspiration begins due to negative pressure created inside the chest cavity by the contraction of the diaphragm. Expiration is a passive process where the air flow occurs due to the elastic recoil property of the lungs. The post-expiratory pause is caused when there is equalization of the pressures inside the lungs and the atmosphere. Breathing cycle is defined as the time interval between the beginning of inspiration and the end of post-expiratory pause. Our method lumps together inspiration and post-expiratory pause, since the thermal signatures of these two are almost identical (Fig. 1).

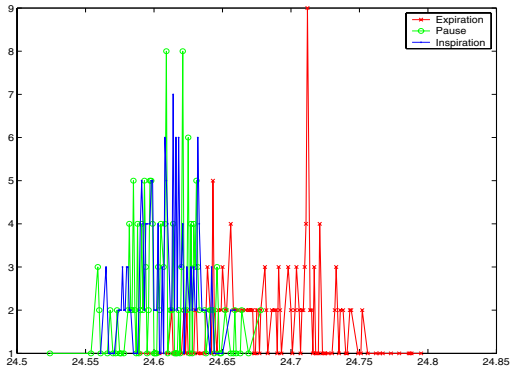


Fig. 1. Typical temperature distributions for the three breathing phases: expiration, post-expiratory pause, and inspiration.

## III. Segmenting and Tracking the Region of Interest

First, we segment skin from no-skin regions using Otsu's adaptive thresholding algorithm [13]. Since we image the profile view of a subject, we consider the tip of the nose the as rightmost point of the facial skin region. A point at a certain distance from the nose tip is taken as an anchor point for the region of interest (ROI) $R$. For our application scenario (50 mm lens and subject at 6-8 feet) we have found experimentally that a region $R$ of $21 \times 9$ pixels gives good results (see Fig. 2). The statistical computation applies within this region only.

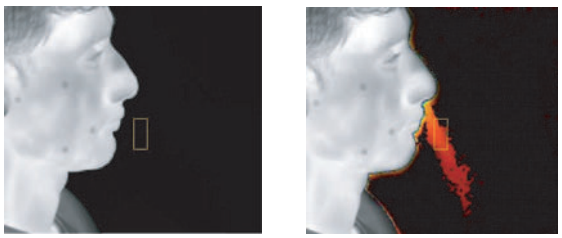

(a) (b)

Fig. 2. Visualization and ROI selection in the air flow region for (a) inspiration and (b) expiration.

## IV. Statistical Methodology

Our methodology includes two distinct phases: training and testing. Training is performed on an individual basis. In the region of interest $R$, we monitor the temperatures during the first few breathing cycles. Specifically, during training the user marks the frames that belong to a full breathing cycle (inspiration + expiration). The marking is real-time thanks to an appropriately designed Graphical User Interface (GUI) and is based on feedback from our visualization algorithm. Our software computes the mean temperature $\bar{T}_k$ in the region $R$ for every frame $k$ of the training sequence. Then, it indexes the maximum $\bar{T}_{k_{max}}$ and minimum $\bar{T}_{k_{min}}$ mean values as well as the mean value $\bar{T}_{(k_{max}+k_{min})/2}$ that lies midway in the timeline between the two. We consider all the temperature values lying between $\bar{T}_{k_{min}}$ and $\bar{T}_{(k_{max}+k_{min})/2}$ in the timeline as the inspiration distribution. We also consider all the temperature values lying between $\bar{T}_{(k_{max}+k_{min})/2}$ and $\bar{T}_{k_{max}}$ in the timeline as the expiration distribution. Furthermore, we consider that the inspiration and expiration distributions are Normal and compute their means and variances accordingly. We repeat this process for two more full breathing cycles and average the inspiration and expiration means and variances for all three training cycles.

During the testing phase we represent at time $t$ each pixel $\mathbf{x}_t$ in region $R$ as a mixture of two distributions:

$$f(\mathbf{x}_t) \sim \pi_{i,t} N(\mu_{i,t}, \sigma^2_{i,t}) + \pi_{e,t} N(\mu_{e,t}, \sigma^2_{e,t}) \quad (1)$$

where,

$$\pi_{i,t} + \pi_{e,t} = 1. \quad (2)$$

$N(\mu_{i,t}, \sigma^2_{i,t})$ is the Normal inspiration distribution, $N(\mu_{e,t}, \sigma^2_{e,t})$ is the Normal expiration distribution, and $\pi_{i,t}$ and $\pi_{e,t}$ are their respective weights in the mixture.

In the beginning of the testing phase ($t = 0$) the distributions for inspiration and expiration are equiprobable $\pi_{i,0} = \pi_{e,0} = 0.5$ and are parameterized by the respective means and variances that we computed during the training phase. Therefore, every pixel in region $R$ is represented as having the following starting distribution:

$$f(\mathbf{x}_0) \sim 0.5 N(\mu_{i,0}, \sigma^2_{i,0}) + 0.5 N(\mu_{e,0}, \sigma^2_{i,0}) \quad (3)$$

At time $t > 0$ and for pixel $\mathbf{x}_t$ we compare the incoming temperature value from the sensor with the available distribution from the previous frame at time $t-1$. For this comparison to be effective we consider that the incoming temperature $\theta_{\mathbf{x}_t}$ can be associated to a Normal distribution $g_t$ with mean $\mu_{g,t} = \theta_{\mathbf{x}_t}$ and variance $\sigma^2_{g,t}$ equal to the square of the camera's sensitivity.

We compute the Jeffrey's divergence measures [12] between the incoming distribution $g_t$ and the available inspiration $f_{i,t-1}$ and expiration $f_{e,t-1}$ distributions respectively. Specifically:

$$J(f_{i,t-1}, g_t) = \frac{1}{2}\left(\frac{\sigma_{i,t-1}}{\sigma_{g,t}} - \frac{\sigma_{g,t}}{\sigma_{i,t-1}}\right)^2 + \frac{1}{2}\left(\frac{1}{\sigma^2_{i,t-1}} + \frac{1}{\sigma^2_{g,t}}\right)(\mu_{i,t-1} - \mu_{g,t})^2 \quad (4)$$

and

$$J(f_{e,t-1}, g_t) = \frac{1}{2}\left(\frac{\sigma_{e,t-1}}{\sigma_{g,t}} - \frac{\sigma_{g,t}}{\sigma_{e,t-1}}\right)^2 + \frac{1}{2}\left(\frac{1}{\sigma^2_{e,t-1}} + \frac{1}{\sigma^2_{g,t}}\right)(\mu_{e,t-1} - \mu_{g,t})^2. \quad (5)$$

We consider that the incoming distribution is closer to the available distribution that features the minimum Jeffrey's divergence measure. We call this the winning distribution $f_{w,t-1}$ and the other the losing distribution $f_{l,t-1}$. Based on this information we update the parameters of the mixture following the method of moments. Specifically, we update the weights for both distributions and the mean and variance of the winning distribution. The mean and variance of the losing distribution remain the same.

The weights of the winning and losing distribution are updated as follows:

$$\pi_{w,t} = (1-\rho)\pi_{w,t-1} + \rho, \quad (6)$$

$$\pi_{l,t} = (1-\rho)\pi_{l,t-1}. \quad (7)$$

The mean and variance of the winning distribution are updated as follows:

$$\mu_{w,t} = (1-\rho)\mu_{w,t-1} + \rho\mu_{g,t}, \quad (8)$$

$$\sigma^2_{w,t} = (1-\rho)\sigma^2_{w,t-1} + \rho\sigma^2_{g,t} + \rho(1-\rho)(\mu_{g,t} - \mu_{w,t-1})^2. \quad (9)$$

The parameter $\rho$ is a learning parameter that is computed from the following formula [14]:

$$\rho = e^{-\frac{1}{2}\left[\frac{\frac{1}{2}(\mu_{g,t}-\mu_w)}{\sigma_w}\right]^2}. \quad (10)$$

The pixel $\mathbf{x}_t$ is given the label of the distribution with the highest updated weight. A count is kept of the number of inspiration $C_{i,t}$ and expiration $C_{e,t}$ pixels in region $R$ at time t. If $C_{i,t} > C_{e,t}$ the frame is labelled as inspiration. Otherwise, the frame is labelled as expiration. Once the first full cycle is detected, the breathing rate is computed using the time stamps of all the frames in the cycle. From that point on the breathing rate is continuously updated every time a breathing cycle is completed. The software displays the breathing rate in cycles/min.

## V. Experimental Setup

We used a cooled mid-wave infrared Phoenix camera with a spectral range of 3.0-5.0 $\mu$m (Indigo, Goleta, CA). The FPA of the camera is $640 \times 512$ and has thermal sensitivity of $0.025^0C$. We used an external black body (Santa Barbara Infrared, Santa Barbara, CA) to calibrate the camera in the temperature range 28.0 - 38.0 $^oC$. We recorded data in a dimly lit room to avoid problems with reflections. Infrared video frames were acquired at a rate of 31 frames per second.

We captured the profile view of the subjects' face from a distance of 6-8 feet. A piezo strap transducer wrapped around the subject's diaphragm was measuring the thoracic circumference during inspiration and expiration and was sending the signal to a PowerLab/4SP vital signs monitor (ADI Instruments, Australia). This was the gold standard that we used for ground truth.

TABLE I

Comparison of computed and ground truth breathing rate.

| Subject Number | Ground Truth Rate | Computed Rate | % Accuracy |
|---|---|---|---|
| 1 | 29.29 | 29.80 | 98.25 |
| 2 | 33.7 | 36.68 | 91.15 |
| 3 | 24.91 | 24.29 | 97.02 |
| 4 | 35.15 | 37.11 | 94.42 |
| 5 | 14.51 | 16.85 | 83.87 |
| 6 | 12.9 | 13.53 | 95.11 |
| 7 | 17.59 | 20.09 | 85.78 |
| 8 | 19.35 | 20.45 | 94.31 |
| 9 | 12.88 | 14.50 | 87.47 |
| 10 | 17.58 | 18.87 | 92.66 |

## VI. Experimental Results

We recorded thermal video clips of 10 subjects during rest and after a light and moderate exercise regime. We have compared the average breathing rate from the ground truth data with that from the computed values and found that our breathing rate computation algorithm conforms to the ground truth rate at 92% (see Table I).

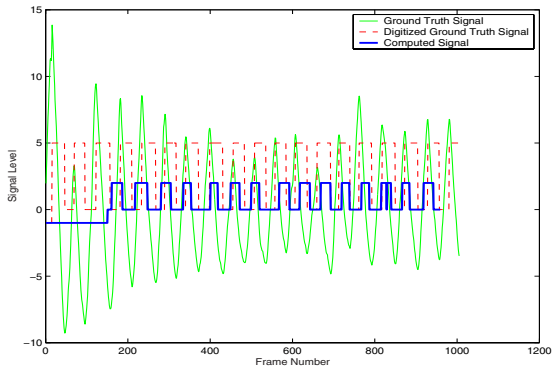


Fig. 3. Comparison of the ground truth and computed breathing signals.

The ground truth signal has output proportional to the expansion (signal rise) and relaxation (signal fall) of the breathing monitor belt during inspiration and expiration respectively. The computed signal has output labelled as either inspiration or expiration. To make comparison between ground truth data and algorithmic results easier, we have digitized both signals by assigning a zero level signal to inspiration and a positive level signal to expiration. In addition, we have assigned a negative signal level to frames used for acquiring training data. Fig. 3 shows the comparison between the ground truth and computed signals. As one can observe, there is phase shift between the two signals. Three primary factors account for this phase shift:

1) Imperfect (manual) synchronization of the beginning of the two recordings (infrared video and monitor belt).
2) The monitor belt records ground truth data at the diaphragm level while our algorithm classifies air flow at the nasal-mandibular level.
3) There is a mismatch of recording frequencies. Our infrared camera records at 31 frames per second while the monitor belt samples at 100 times per second.

We have countered the third factor by averaging three consecutive ground truth samples for every video frame. We have countered the first two factors by shifting the computed signal by the necessary amount.

## VII. Conclusion

In conclusion, breathing function is one of the major indicators of an individual's health. It can be used to predict various life threatening disorders like sudden infant death syndrome and heart attacks. It is also used in sleep studies to detect sleep apnea. Finally, it is one of the psycho-physiological channels in polygraph examinations. Various modalities have been developed to measure breathing rate. Almost all the legacy methods require contact and hence they compromise the subject's comfort and mobility. Moreover, measurements by these methods are corrupted either by movement artifacts or by their dependence on other physiological variables, like heart rate. We have proposed a method that is based on infrared imaging and statistical computation to measure passively breathing rate at a distance. The method has the potential to provide a unique capability for sustained monitoring of chronic or acute breathing problems by overcoming the deficiencies of the existing measurement modalities. It also opens the way for the next generation touchless polygraphy that will not affect the subject's psycho-physiology.

## VIII. Acknowledgements

This research was supported by DARPA grant $\#N00014-03-1-0622$ and by the University of Houston start-up funds of Professor I. Pavlidis. The views expressed in this paper do not necessarily reflect the views of the funding Agencies. We are thankful to Dr. Ralph Chatham at DARPA for his valuable help.

## References

[1] Moody G.B., Mark R.G., Bump M.A., Weinstein J.S., Berman A.D., Mietus J.E., and Goldberger A.L., *Clinical Validation of the ECG-Derived Respiration (EDR) Technique*, Computers in Cardiology, Vol. 13, pp. 507-510, 1986.

[2] Kim T. and Khoo M.C.K., *Estimation of Cardiorespiratory Transfer Under Spontaneous Breathing Conditions: A Theoretical Study*, The American Journal of Physiology, Vol. 273, No. 2, pp. H1012-H1023, August 1997.

[3] Partinen M., Alihanka J., and Hasan J., *Detection of Sleep Apneas by the Static Charge-SensitiveBed*, 6th European Congress on Sleep Research, Zurich, March 1982.

[4] Larson B.H., *Signal Processing Techniques for Non-Invasive Monitoring of Respiration and Heart Rate*, University of Houston, 1987.

[5] Storck K., Karlsson M., Ask P., and Loyd D., *Heat Transfer Evaluation of the Nasal Thermistor Technique*, IEEE Transactions on Biomedical Engineering, Vol. 43, No. 12, pp. 1187-1191, December 1996.

[6] Nepal K., Biegeleisen E., and Ning T., *Apnea Detection and Respiration Rate Estimation Through Parametric Modeling*, Proceedings of the 28th IEEE Annual Northeast Bioengineering Conference, Philadelphia, Pennsylvania, April 2002.

[7] Barschdorff D. and Zhang W., *Respiratory Rhythm Detection with Plethysmographic Methods*, Engineering Advances: New Opportunities for Biomedical Engineers, Vol. 2, pp. 912-913, November 1994.

[8] Greneker E.F., *Radar Sensing of Heartbeat and Respiration at a Distance with Applications of the Technology*, RADAR 97, No 449, 150-154, October 1997.

[9] Pavlidis I., Levine J., and Baukol P., *Thermal Imaging for Anxiety Detection*, Proceedings of the 2000 IEEE Workshop in Computer Vision Beyond the Visible Spectrum: Methods and Applications, pp. 104-109, Hilton Head Island, South Carolina, June 16, 2000.

[10] Pavlidis I., Eberhardt N.L., and Levine J., *Human Behavior: Seeing Through the Face of Deception*, Nature, Vol. 415, No. 6867, January 3, 2002.

[11] Silverthorn D.U., *Respiratory Physiology*, Human Physiology: An Integrated Approach, 2nd Edition, pp.498-508, Prentice-Hall, Inc., 2001.

[12] Pavlidis I., Morellas V., Tsiamyrtzis P., and Harp S., *Urban Surveillance Systems: From the Laboratory to the Commercial World*, IEEE Proceedings, Vol. 89, No. 10, pp. 1478-1497, October 2001.

[13] Otsu N., *A Threshold Selection Method from Gray-Level Histograms*, IEEE Transactions on Systems, Man, and Cybernetics, Vol. 9, No. 1, pp. 62-65, 1979.

[14] Pednekar A., Kakadiaris I.A., and Kurkure U., *Adaptive Fuzzy Connectedness-Based Medical Image Segmentation*, In Proc. of the Indian Conf. on Computer Vision, Graphics, and Image Processing (ICVGIP'02), pp.457-462, Ahmedabad, India, December 16-18, 2002.